Chapter 4

Application of WO_3 as alternative photoanode material for Dye Sensitized Solar Cells

This Page is intentionally left blank

4.1. Introduction

Increasing energy demand and environmental contamination are the two major problems faced by society in recent years. The major energy requirements of the world are fulfilled by fossil fuels (i.e., coal, petroleum and natural gas), which may not be sufficient to overcome the energy crisis in the future due to fast depletion, the rapid development of industrialization and environmental pollution[1-4]. To address these issues, scientists have focused on renewable and environment-friendly energy sources. As Sun represents an immense source of renewable energy, expected to provide an appreciable amount of power in the future, it is the most widespread type of alternative energy source among all the renewable energy sources [5-7]. Dye-sensitized solar cells, an unconventional photoelectrochemical device that directly converts photo-energy into electrical energy, have drawn much more attention than conventional silicon solar cells due to their easy fabrication technique, the low-level requirement of the high-temperature process, cost-effectiveness and environment-friendly nature [8, 9]. But until now, DSSCs are not commercially viable as the reason for their comparatively low conversion efficiency and stability issues compared to the silicon-based solar cells [10]. Photo anode, the heart of a DSSC system plays a key role in enhancing the overall performance of the DSSC by transferring electrons and supporting the Dye molecules [11]. It consists of a nanostructured mesoporous semiconductor film deposited on a conducting glass or a flexible substrate [12, 13]. An ideal photoanode material should have some properties of high charge carrier mobility, significantly high surface areas, environmental friendliness, cost-effectiveness, and comparatively less electron-hole recombination rate. The band edge positions and corresponding band gap values of several commonly used wide bandgap metal oxide semiconductors are shown in Fig. 4.1 [14, 15]. The semiconducting oxide material TiO_2 is mostly used as a photoanode because of

its excellent optical, electrical and chemical properties [16-19]. Although appreciably high

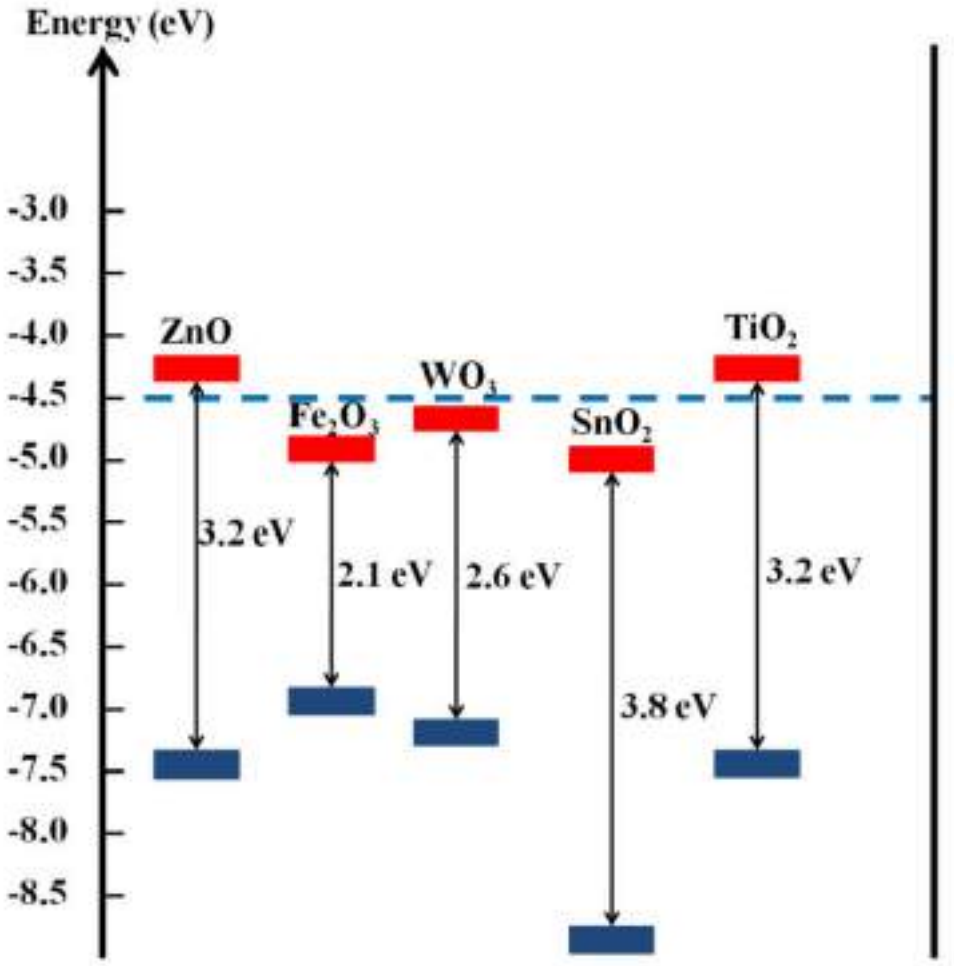

Figure 4.1 Energy band positions of several semiconductors.

conversion efficiency is achieved with TiO_2, its low electron mobility leads many scientists to think about new alternative photoanode materials for better performance of Dye sensitized solar cells [20]. On the other hand, WO_3, a wide bandgap semiconductor having bandgap in the range of 2.6eV-3.1eV has been used extensively in the fabrication of gas sensors, water splitting and photocatalyst [21]. Owing to the favourable bandgap, high electron mobility and extreme stability in harsh environments, it has attracted the attention of researchers as an alternative photoanode material for DSSC fabrication.

Moreover, the nonreactive nature of WO_3 in acidic environments may provide the solution of long-term stability issues in DSSCs with more acidic electrolytes. However, DSSCs based on pure WO_3 photoanode have been proven to be inefficient. On the other hand, DSSCs based on surface modified WO_3 photoanode by ultrathin layer of TiO_2 exhibited significant increase in power conversion efficiency [22]. ZnO can be used as a substitute for TiO_2 due to its agreeable properties in the view of high electron mobility and abundant nanostructure morphologies [23-25]. To the best of our knowledge, however, there are no detailed reports found in which surface modification of WO_3 is done by an ultrathin layer of ZnO in the fabrication of DSSCs. In this work, we have prepared the WO_3 photoanode and a facile sol-gel spin coating technique was utilized to alter the surface property of it by a thin layer of ZnO. Very careful control of the thickness of the ZnO layer is necessary to get the optimum performance out of the solar cell and for this purpose different concentration of ZnO precursor solution was used.

4.2. Materials and Method

4.2.1. *Preparation of working electrodes*

All the reagents used in the fabrication process were of analytical grades. So no further purification was required. To prepare the thin films of the photoanode materials, the ITO coated glass substrates were first cleaned with dilute HCl in an ultrasonic bath for 15 minutes and then thoroughly rinsed with deionized water to remove the HCL residues. Then the substrates were cleaned with acetone and ethanol using an ultrasonic cleaning bath [26].

The working electrode of the DSSC was prepared by following the standard doctor blade method. The WO_3 paste for doctor blading was prepared by mixing WO_3 nanopowder with terpineol as solvent and ethyl cellulose as a binder and stirred continuously in order to obtain a smooth lump-free slurry.

The WO_3 paste was then coated on the conductive side of the cleaned ITO glass substrate and subsequently annealed at 500^oC for 2 hr in order to burn out the terpineol and ethyl cellulose contents of the working electrode and strengthens the bonding between the substrate the WO_3 film. In addition to this, the annealing procedure also helps to improve the surface quality of the thin film along with increasing the crystallinity of the sample [22].

The Sol-Gel spin-coating technique was employed to deposit thin layers of ZnO onto the surface of the as-prepared WO_3 photo-anode. Zinc acetate dihydrate $(CH_3COO)_2 Zn, 2H_2O$, (98% Merck) was mixed with acetone at different molar ratios to obtain desired concentrations of ZnO precursor solution. The prepared solutions were then mixed extensively in an ultrasonic bath for 2 hours and then spin-coated on the WO_3 coated substrate using a programmable spin coater (Apex Instruments Co. Pvt. Ltd, Model SpinNXG-P1) at 2000 rpm for 30 seconds. The thickness of the ZnO film can be controlled by varying the precursor solution concentration. In our experiment we have prepared 1 mM, 5 mM, 10 mM, 15 mM, 20 mM, and 25 mM solutions of ZnO precursor and spin-coated them over WO_3 film keeping the number of sol drops unchanged in order to obtain various ZnO film thickness and study the effect on the solar cell performance. The ZnO coated WO_3 electrode was annealed at 450^oC for 1 hour. All the electrodes were sensitized by immersing them in a 0.3 mM ethanolic solution of Ruthenium based dye ($C_{26}H_{20}O_{10}N_6S_2Ru$) known as N_3 (Solaronix) for 48 hours. The working electrodes were then removed from the solution and thoroughly rinsed with deionized water and ethanol to remove any excess dye from the semiconductor film surface and air-dried at room temperature.

The counter electrodes of the cells were prepared by spin coating the platinum catalyst precursor solution Platisol-T (Solaronix) on the conducting side of the cleaned ITO coated glasses and heating on a hot plate at 450 ^{o} C for 15 minutes.

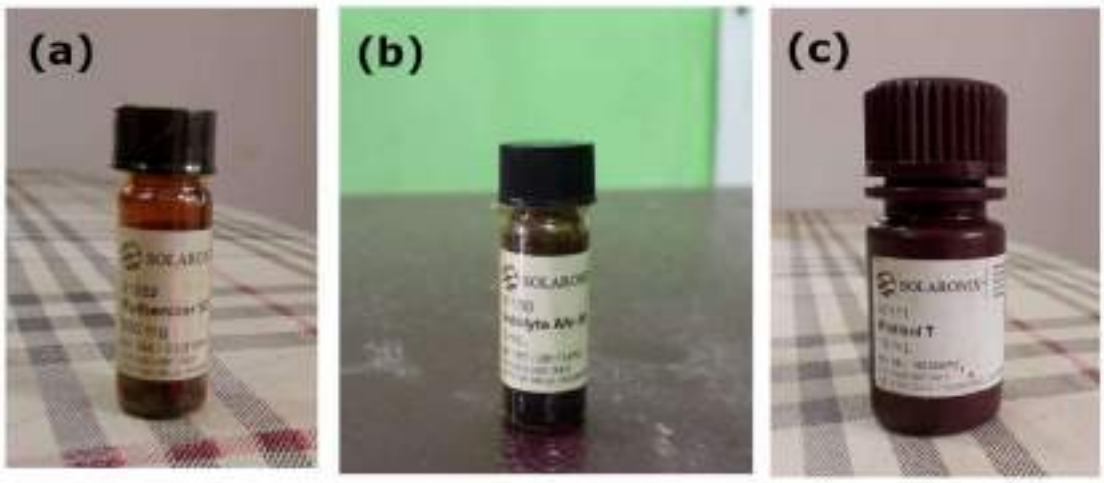

Figure 4.2 (a) N3 dye, (b)Iodolyte AN50 electrolyte, (c) Platisol T used for preparing Pt counter electrode in DSSC fabrication.

Figure 4.3 DSSC fabricated with N3 dye and WO_3 as photoanode material.

The dye adsorbed working electrode and Pt- coated counter electrode was assembled against the coated sides of each other in a sandwich manner using two binder clips with a Surlyn film (Meltonix 1170-25µm, Solaronix) gasket as a spacer in between them. The liquid electrolyte used in our experiment was a Solaronix high-performance electrolyte (Iodolyte AN50) with iodide/tri-iodide as redox couple, ionic liquid, and lithium salt and pyridine derivative as additives dissolved in acetonitrile solvent. The redox concentration of the electrolyte was 50 mM. The active area of the cells for

illumination was determined by employing a black mask of aperture size 0.25 cm^2.

4.2.2. *Characterization and Measurements*

The crystalline structure of the WO3 and ZnO were analyzed with the help of X-ray diffraction analysis using the PAN-analytical X'Pert PRO X-ray diffractometer (CuKα radiation, 30 mA, 40 kV, λ= 1.5406 Å). Scanning electron microscopy (JEOL) was done to reveal the surface morphology of the prepared thin films. More detailed structural information of the samples was obtained from Raman Spectroscopy. The Photocurrent-Voltage (I-V) characteristics data of the cells were recorded using Keithley 2400 digital source meter with the help of a computer under 100 mW/cm^2 illumination (Xenon lamp 450W). HIOKI Impedance Analyzer in the frequency range of 0.1Hz to 190 kHz was used to study the electrochemical impedance spectra of the cells.

4.3. Results and Discussion

4.3.1. *Structural and phase characterization WO_3 photoanode*

Figure 4.3. shows the X-ray diffraction pattern of the as-purchased WO_3 nanopowder. The XRD pattern exhibits the coexistence of both the monoclinic and orthorhombic crystal phases. The peaks corresponding to the monoclinic phase well matches with the standard JCPDS card no. 43-1035 and the orthorhombic phase matches with JCPDS card no. 20-1324. Sharp and strong peaks signify the high crystalline nature of the sample [27, 28].

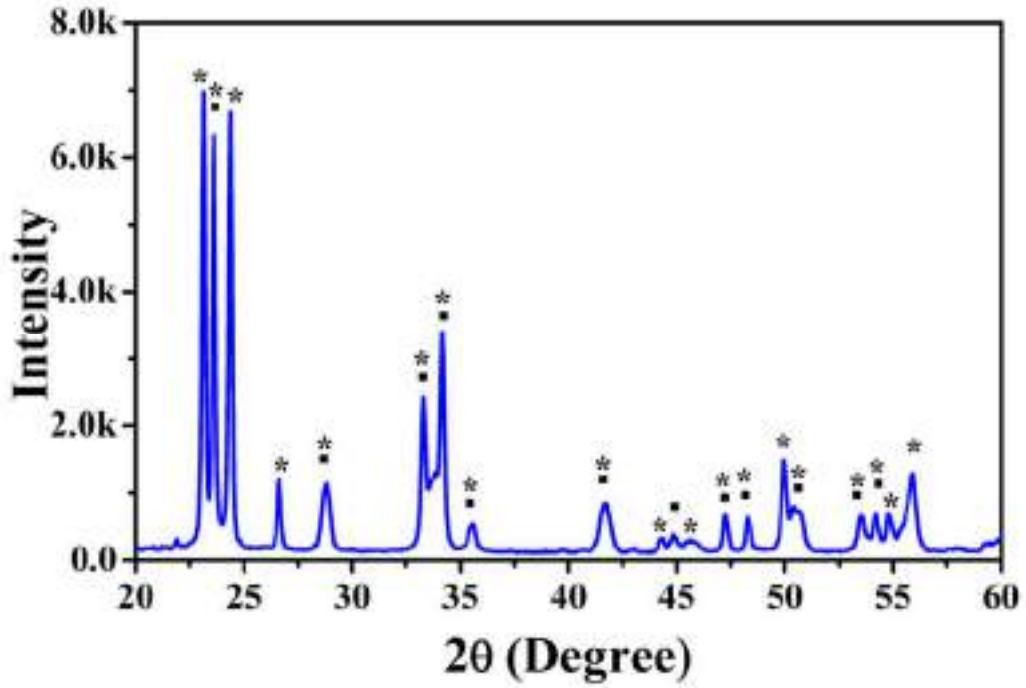

Figure 4.4 X-ray diffraction pattern of WO_3 nanoparticles. The peaks correspond to Monoclinic (*) and orthorhombic (▪) phases of WO_3 respectively.

The crystal phases are further confirmed by Raman spectra of the pure WO_3 powder, which is shown in fig. 4.3 and it consists of well-resolved four sharp Raman peaks at 274, 329, 719 and 807 cm^{-1}. The lower peaks centered at 274 cm^{-1} and 329 cm^{-1} attributed to O-W-O bending vibrations and the higher peaks at 719 cm^{-1} and 807 cm^{-1} are due to W-O-W stretching mode vibration [29]. Sharp peaks suggest profoundly crystalline nature of the sample. All four Raman peaks attribute to the monoclinic phase [30]. However, the Raman peaks corresponding to the orthorhombic phase lie neighbouring to the peaks mentioned above. Consequently, both phases are believed to be present in the sample. No impurity was found in the Raman spectra of the pure WO_3 sample.

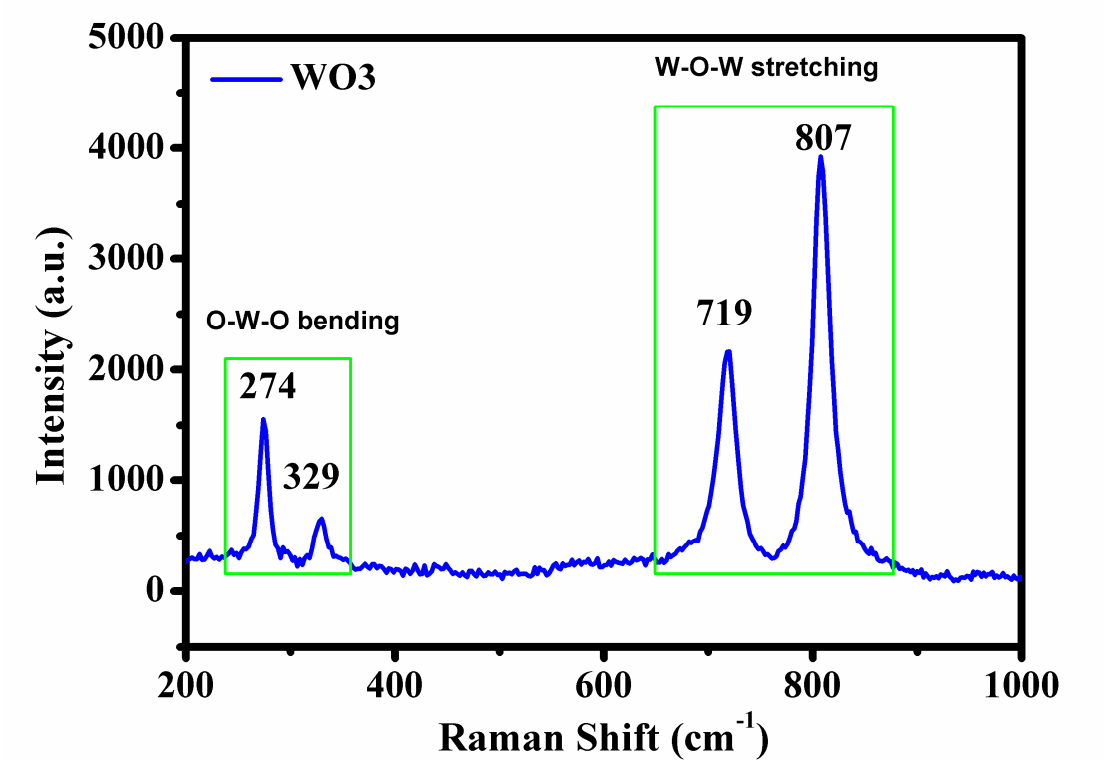

Figure 4.5 Raman spectra of WO_3 nanoparticle.

4.3.2. *Surface Morphology study and energy dispersive spectroscopy of the photoanodes*

Scanning Electron Microscopy was employed to investigate the surface morphology of the pure and ZnO coated WO_3 photoanodes. Fig. 4.4(a) shows the SEM image of pure WO_3 photoanode on the FTO substrate whereas Fig. 4.4(b-g) show the SEM images of WO_3 photoanodes coated with 1mM, 5mM, 10mM, 15mM, 20mM and 25mM concentrations of ZnO precursor solution concentrations respectively. Highly porous films with nearly spherical shape WO_3 nanoparticle having a diameter in the range of 140nm-150nm can be clearly seen from the SEM images. High porosity the film enhances the surface

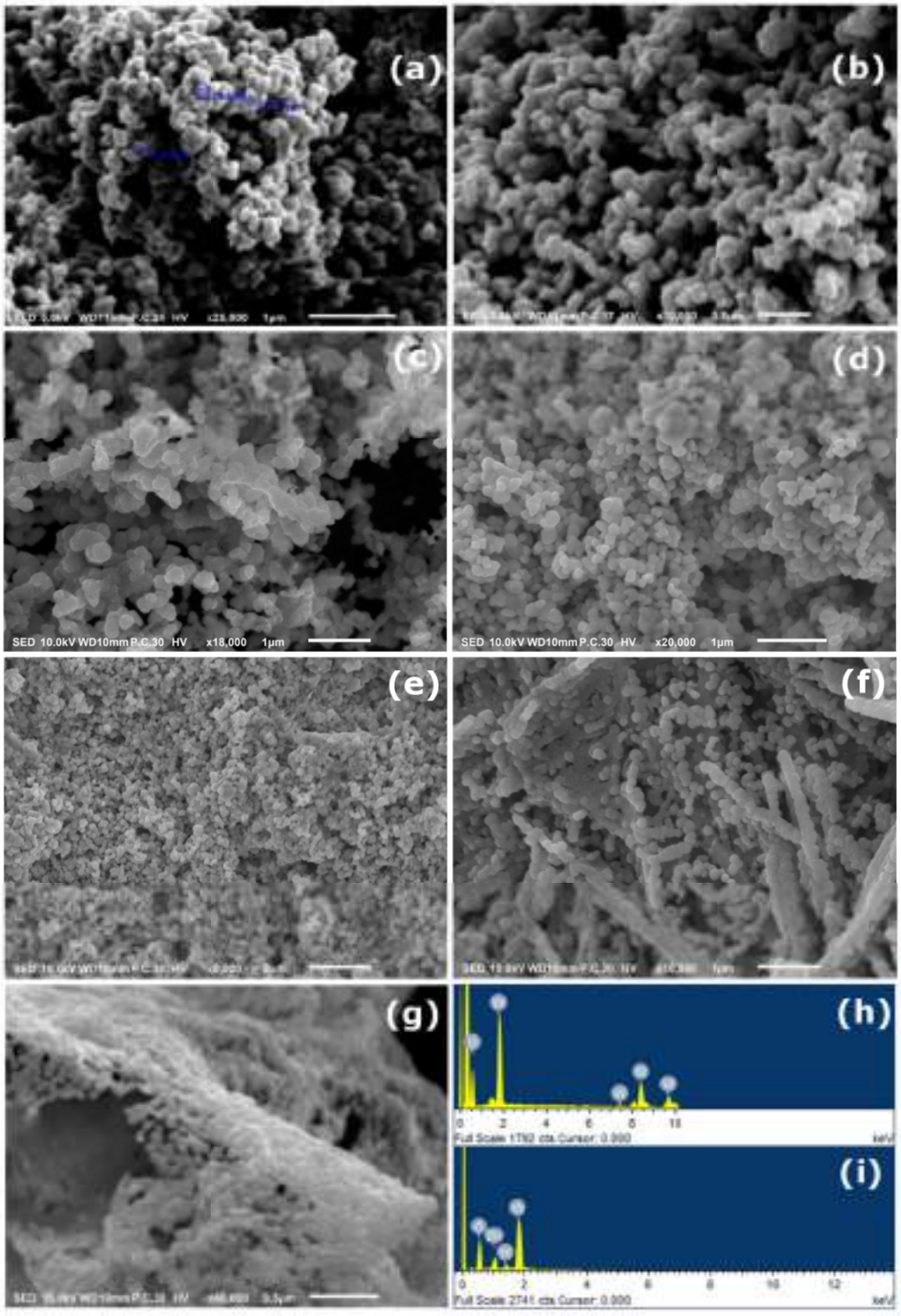

Figure 4.6 SEM images of (a) Bare WO_3 photoelectrode ; photoelectrodes having WO_3 coated with (b) 1mM (c) 5mM (d) 10mM (e) 15mM (f) 20mM and (g) 25mM ZnO precursor solution respectively. (h) EDS of Bare WO_3 and (i) EDS of WO_3 coated with 5mM ZnO.

to volume ratio, consequently increasing the dye loading amount resulting in high photocurrent [31-34]. It can also be observed from the SEM images that the surface morphology of uncoated and ZnO coated WO_3 substrate are not so visually different for low ZnO precursor concentrations, but for higher concentrations like 20 mM and 25 mM, the screening of WO_3 surface by ZnO nanoparticles may be evidently observed in Fig. 4.4(f) and 4.4(g).

The EDS spectrum, which reveals the elementary analysis are shown in fig. 4.4(h) and 4.4(i) for bare WO_3 and the WO_3 surface coated with 5mM ZnO precursor solution concentration respectively. Predominating peaks of W and O_2 in Fig. 4.4(h) unveil that the sample contains only WO_3 whereas in Fig. 4.4 (i) additional strong peak of Zn confirms the presence of ZnO coating over WO_3.

4.3.3. *Current-Voltage characterization of the cells*

The Current-Voltage characteristic is a crucial characterization to investigate the overall photovoltaic performance of a solar cell. Fig. 4.5(a) illustrates the I-V characteristics of the seven DSSCs based on pure and coated WO_3 as photoanodes with different precursor solution concentrations. The overall photoconversion efficiency of the solar cell is given by

$$\eta = \frac{P_{out}}{P_{in}} = \frac{I_{sc}V_{oc}FF}{P_{in}} \qquad (1)$$

Where I_{sc}, V_{oc}, FF and Pin represent the short circuit current density , open-circuit voltage,Fill factor and incident light power respectively light power respectively. The fill factor is calculated by the formula

$$FF = \frac{I_{max}V_{max}}{I_{sc}V_{oc}} \qquad (2)$$

Where V_{max} and I_{max} are the voltage and current corresponding to the maximum output power point of the solar cell respectively. All the photovoltaic parameters obtained from the I-V curve are summarized in Table 4.1.

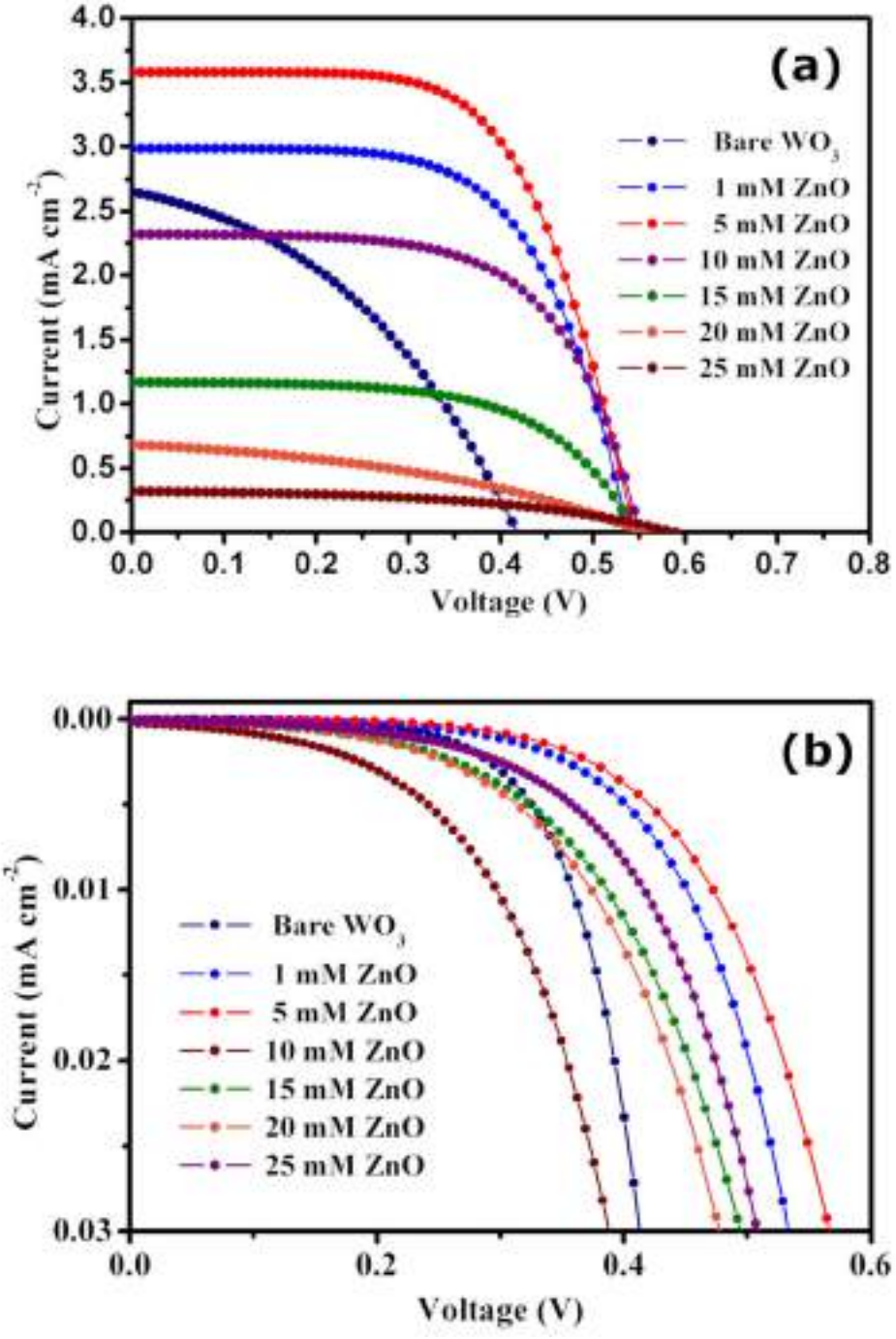

Figure 4.7 Current-voltage characteristics of different cells under (a) Illumination and (b) Dark.

A clear enhancement in the efficiency and fill factor due to the presence of ZnO on the WO_3 surface compared to the bare WO_3 electrode can be observed from Table 4.1. The fill factor, which represents the squareness of the I-V curve [35], is very low for bare WO_3 which in turn decreases cell efficiency. The low fill factor may be attributed to the high recombination rate of electrons for bare WO_3 photoelectrode DSSC. However, a significant improvement in the value of J_{sc} can be noted from table 4.1 upon ZnO coating over the WO_3 surface which demonstrates the positive role of the ZnO layer in reducing the recombination process. The DSSC with 5 mM ZnO precursor solution concentration yielded the highest short circuit photocurrent J_{SC} and efficiency η. But the photocurrent and the efficiency start falling sharply with a further increase in the precursor solution concentration.

Table 4.1. Photovoltaic performance of uncoated and ZnO coated WO_3 photoanode based DSSC.

ZnO precursor solution concentration	J_{sc} (mA/cm^2)	V_{oc} (V)	FF	Efficiency (η %)
Pure WO3	2.65	0.42	0.39	0.44
1 mM ZnO	2.98	0.53	0.63	1.07
5 mM ZnO	3.58	0.55	0.62	1.21
10 mM ZnO	2.32	0.56	0.62	0.80
15 mM ZnO	1.67	0.56	0.60	0.38
20 mM ZnO	0.68	0.57	0.38	0.15
25 mM ZnO	0.32	0.58	0.47	0.09

The maximum value of open-circuit voltage is determined by the difference between the Fermi level of the photoanode (metal oxide) material and the red-ox potential of the liquid electrolyte [36]. WO_3 is known to possess a lower conduction band edge (E_{cb}) i.e. more positive E_{cb} thereby reducing the

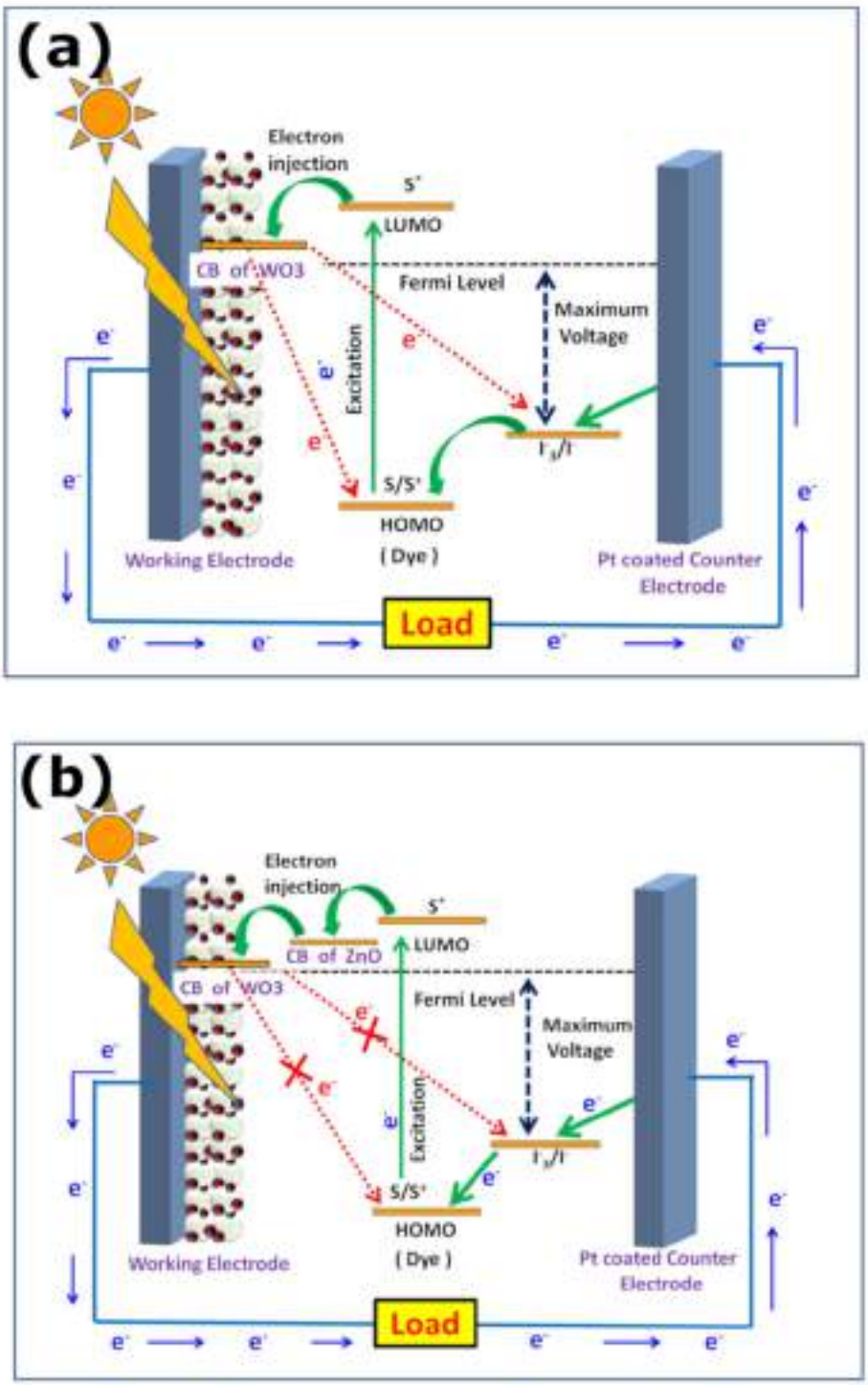

Figure 4.8 Schematic energy level diagram and mechanism of the (a) Conventional DSSC and (b) DSSC with the ZnO barrier.

open-circuit voltage (V_{oc}). However, employing an ultrathin layer of more E_{cb} negative metal oxides like ZnO onto WO_3 surface may increase the value of V_{oc} as the photogenerated electrons from LUMO of dye molecules are now injected to the more negative conduction band of ZnO and then step down to the conduction band of WO_3 which is illustrated in Fig. 4.6 (b).

Furthermore, the energy barrier created due to the incorporation of ZnO onto the WO_3 film surface may prevent the charge carrier recombination and as well as decreasing back transfer of electrons to the HOMO of the dye molecule. Aside from this, the ultrathin layer of ZnO incorporation on the WO_3 surface facilitates the amount of dye adsorption and hence increasing the amount of photon absorption resulting in higher J_{sc}.

The dark current measurement was done in order to interpret the variation of charge recombination reaction of the photogenerated electrons with I_3^- ions at the Pt coated counter electrode/red-ox electrolyte interface. Fig. 4.5(b) shows the dark J-V characteristics of the DSSCs fabricated with uncoated and coated with different concentrations of the ZnO precursor solution. The photoelectron injection from LUMO of dye to the CB of the working electrode is completely absent in the dark condition and hence the dark current is mainly due to the diffusion of electrons from semiconductor to the redox electrolyte [37]. Ultrathin coating of ZnO layer on the WO_3 surface decreases the dark current which can be observed in dark current characteristics in Fig. 4.5(b). On the other hand, the uncoated WO_3 possesses a higher dark current for a particular bias voltage. This may be due to the fact that poor dye loading capacity of WO_3 allows more direct contact between WO_3 surface and liquid electrolyte. This facilitates the back transfer of electrons from WO_3 to electrolyte via reduction of I_3^- into I^- which led to increased dark current [22]. But the coating of ZnO creates an energy barrier that effectively reduces the rate of electron recombination thereby decreasing the dark current, consequently suppressed recombination of charge carriers due to ZnO coating

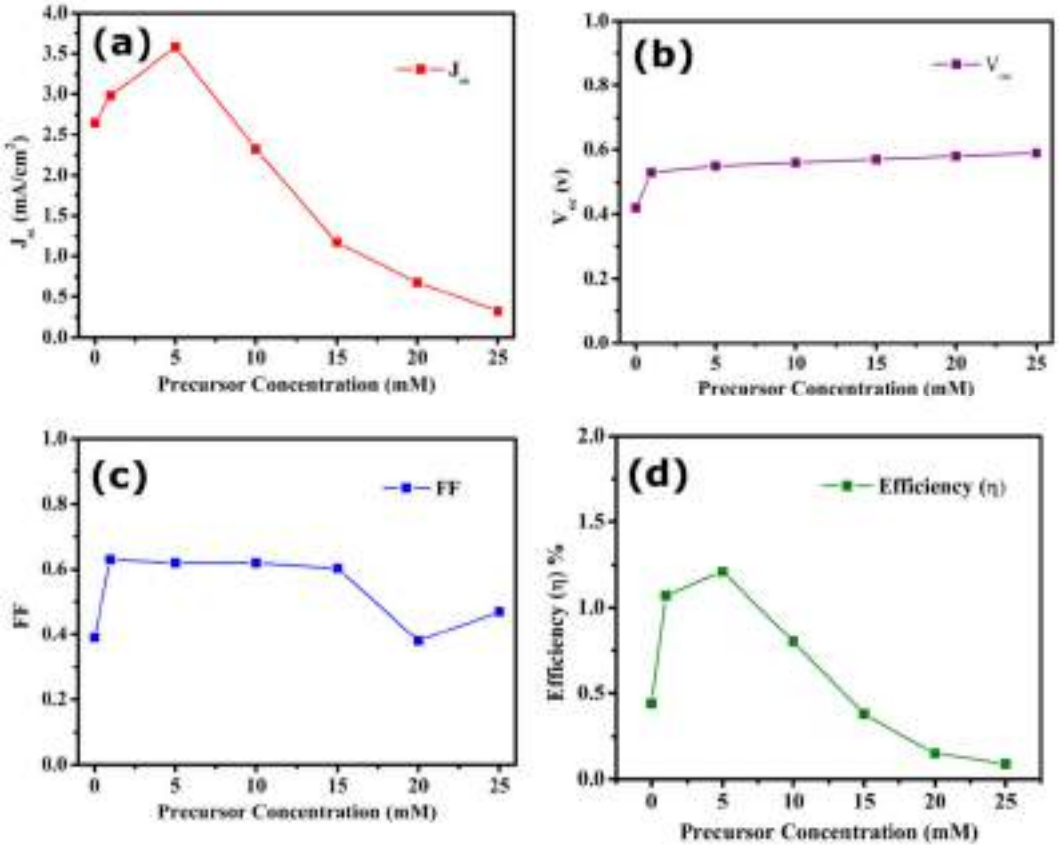

Figure 4.9 Effect of ZnO precursor solution concentration on the values of photovoltaic parameters (a) J_{SC} (b) FF (c) Voc and (d) η.

increases cell FF. In addition to that, a very thin coating of ZnO also improves the dye loading which enables the ZnO treated WO_3 DSSC to harvest more light energy compared to ordinary WO_3 DSSC and significantly enhances current density. However, with the increase in the ZnO precursor concentration of more than 5 mM, the values of FF and J_{sc} start decreasing. This decrease in J_{sc} and FF might be due to the fact that thicker ZnO completely screens WO_3 from dye molecules. Moreover, a higher amount of ZnO content act as recombination sites [38]. Apart from this, an increased amount of ZnO deposition via increasing the ZnO precursor solution concentration promotes aggregation of Zn^{+2} ions and N3 dye which may decrease the photocurrent due

to light loss due to absorption and scattering of light by these aggregates [39-41].

Figure 4.7 shows the variation of the different DSSC performance parameters as a function of ZnO precursor solution concentration. The values of J_{sc}, FF, and η enhanced significantly for the cells with ultrathin ZnO nanoparticles coating as compared to the cell with bare WO_3 nanoparticle thin film. The best performance was obtained with 5 mM ZnO solution concentration with values of cell parameters like J_{sc}, V_{oc}, FF, and η as 3.56 mA/cm^2, 0.55 V, 0.62 and 1.21 % respectively.

4.3.4. *Electrochemical impedance spectroscopy*

Electrochemical impedance spectroscopy was performed to further explore the interfacial charge transport properties and recombination resistances for a better understanding of the cell parameters. The EIS measurement was carried out at V_{oc} bias voltage and applying an AC voltage of 10mV amplitude to the DSSC under 1 sun illumination in the frequency range 0.1 Hz to 190 kHz. The Nyquist plot of the different DSSCs fabricated using bare WO_3 and with a coating of different concentrations of ZnO onto it are depicted in Fig. 4.8(a). Usually, a typical Nyquist plot consists of three semi-circles. The first semicircle in the high-frequency range is attributed to the charge transport resistance at the Pt counter electrode/ electrolyte interface, while the second semicircle in the mid-frequency range represents the recombination resistance at the semiconductor/dye/electrolyte interface. The third semicircle is associated with Nernst diffusion (Warburg diffusion impedance Z_w) which is the impedance faced by the electrons during diffusion through the electrolyte [39]. However, in our case only two semicircles are present as the third semicircle is usually observed at frequencies below 0.1 Hz [42]. The intersection/intercept of the 1^{st} semicircle on the real axis of the Nyquist plot in the high-frequency range represents the sheet resistance of

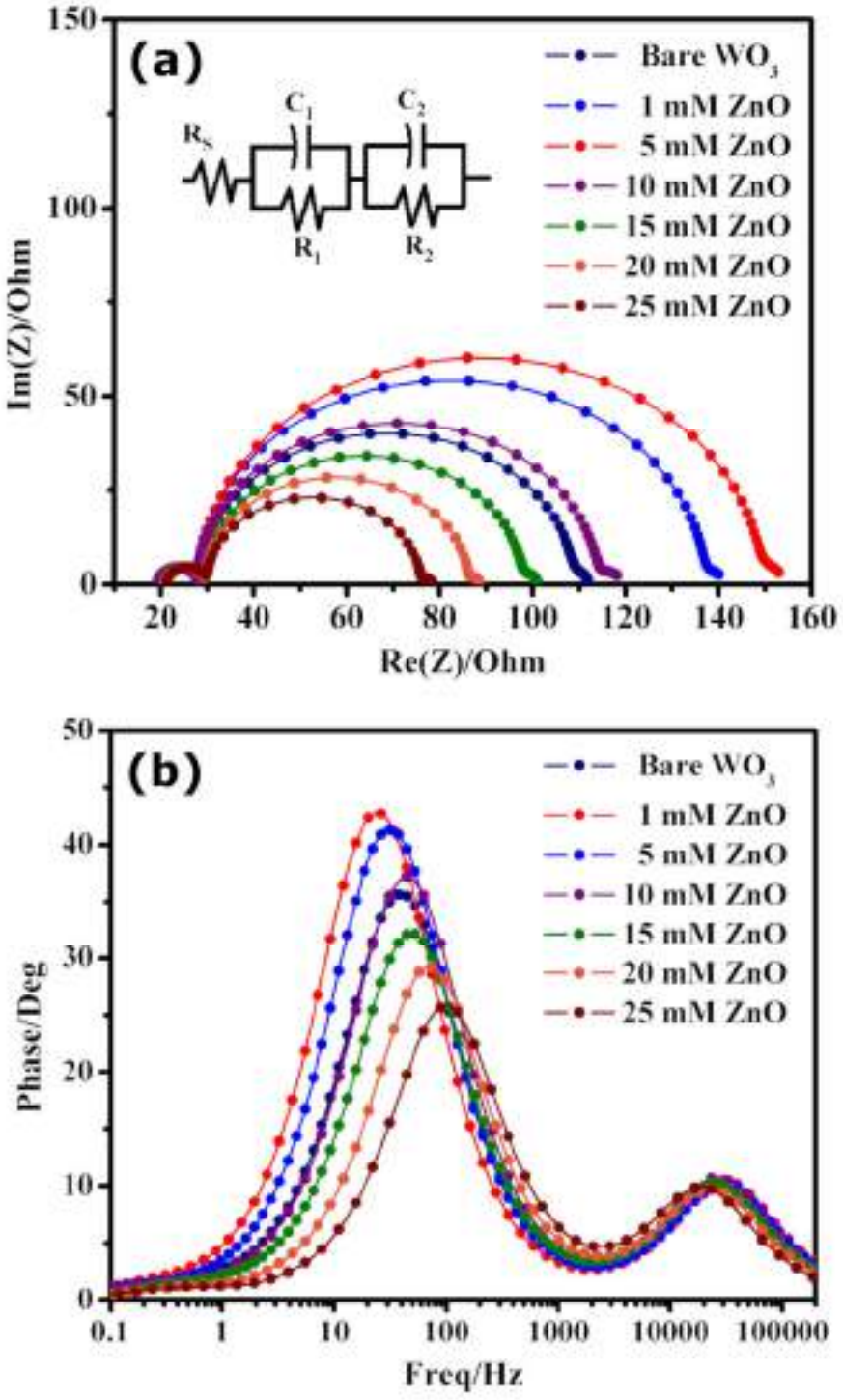

Figure 4.10 Electrochemical Impedance Spectra of the DSSCs (a) Nyquist plot along with equivalent circuit (inset) (b) Bode plot.

FTO and other ohmic contact resistances (R_s) of the assembled cells. The capacitive components C_1 & C_2 in the equivalent circuit are due to the formation of charge double layer between the counter electrode/electrolyte and semiconductor/dye/electrolyte interfaces respectively [43]. The equivalent circuit, shown in the inset of Fig. 4.8(a) is used to fit the experimental Nyquist plot and the obtained EIS parameters are represented in table 4.2. The value of contact resistance (R_s) is almost the same for all the coated cells except the bare WO_3 cell. The increase in the value of R_s in ZnO coated cells may be due to the increase in the number of layers. The value of recombination resistance (R_2) is very low for bare WO_3. But a gradual increase in R_2 with an increase in ZnO precursor concentration may be observed in Fig. 4.8(a) and table 4.2. The highest value of R_2 is observed for 5 mM ZnO concentration as this much concentration provided the highest amount of dye adsorption without affecting the carrier transport through WO_3 thereby generating the highest number of charge carriers and also reducing the charge carrier recombination at the semiconductor/due/electrolyte interface.

Table 4.2. Summary of EIS measurements of the fabricated DSSCs.

ZnO precursor solution concentration	R_S (Ω)	R_2 (Ω)	R_1 (Ω)	C_2 (μF)	Peak freq. f(Hz)	Electron lifetime(τ_e) (ms)
Pure WO3	19.3	85.2	8.67	84.3	37.18	4.28
1 mM ZnO	19.5	108.3	8.4	103.7	31.36	5.08
5 mM ZnO	19.6	119.7	8.62	125.4	24.15	6.59
10 mM ZnO	20.1	79.57	8.36	98.35	40.72	3.91
15 mM ZnO	20.8	67.57	8.79	87.35	48.47	3.29
20 mM ZnO	21.1	56.23	8.41	68.3	68.67	2.32
25 mM ZnO	21.3	45.76	8.52	55.57	97.29	1.64

Further increase in ZnO concentration starts decreasing R_2 due to poor dye loading on the WO_3 surface. Along with that presence of recombination sites for the free charge carriers in the thick layer of ZnO (38). Thick ZnO layer also makes the thickness of the film such a high that it becomes greater than the diffusion length of the electrons. This decreases the net photocurrent reaching the FTO and lowers the cell performance. The highest value of chemical capacitance C_2 also reflects the transformation of a higher amount of photon energy into chemical energy [44, 45]. To estimate the charge carrier lifetime, the Bode plot representing variation in phase angle (θ) with frequency (f) for varying amounts of ZnO concentration is depicted in Fig. 4.8(b). The electron lifetime is calculated using formula [46-49],

$$\tau_n = \frac{1}{2\pi f_{max}}$$

Where f_{max} represents the characteristic peak frequency of the Bode plot in the mid-frequency range. The lower value of f_{max} is associated with a higher electron lifetime. The DSSC with 5mM ZnO coating has the lowest value of f_{max} leading to the highest lifetime of photogenerated electrons. This enhancement in electron lifetime reduces the recombination process leading to the highest photocurrent among the seven fabricated cells in our study. These results are in accordance with the results obtained from J-V characteristics under illumination and dark.

4.4. Conclusion

In this study, we have fabricated DSSCs based on WO_3 as an alternative photoanode material. The DSSC showed an efficiency of 0.44% with a low FF of 0.39. This was due to very high recombination rates of photoexcited electrons along with poor dye loading due to the highly acidic surface of WO_3. Apart from that, the lower conduction band edge position of WO_3 limits the open-circuit voltage of the DSSC. In order to improve the performance of WO_3

based DSSC, the effect of inclusion of the ZnO thin layer on the surface of WO_3 was studied. The current densities (J) – voltage (V) characteristics of the prepared cells were compared and a clear enhancement of cell efficiency was recorded upon ZnO coating and the highest efficiency was achieved for 5 mM concentration. Although the incorporation of a thin layer of ZnO onto WO_3 enhances the power conversion efficiency by creating an energy barrier and limiting the electron back-recombination, the thicker layer of ZnO degrades the cell performance by forming an aggregation of Zn^{+2} ions and N_3 dye and reducing the dye adsorption quantity of WO_3 film. This suggests an optimum concentration for ZnO to be deposited over WO_3 film to achieve the highest efficiency. The improvement of the value of V_{oc} due to ZnO coating was attributed to the upward shift in CB of WO_3. Apart from J-V characteristics, study under illumination and dark, EIS measurement was also performed. It was found that the cell with 5mM of ZnO over WO_3 film has the highest recombination resistance which efficiently retards/suppresses the electron recombination rate and as result, the lifetime of photogenerated electrons is also highest. The decrease in the photoconversion efficiency with further increase in ZnO concentration above optimum value is due to the complete screening of WO_3 film by a thicker layer of ZnO. Therefore, the novel method used here to modify the surface property of the WO_3 photoelectrode of DSSC is found to be promising to enhance the cell performance and thereby develop an efficient WO_3 based Dye sensitized Solar cell.

References:

[1] Bach W. Global warming: the complete briefing (2nd ed). John Houghton. Cambridge University Press: Cambridge, 1997. Pp. xv + 251. Paperback: ISBN 0521-62932-2, ú12.95; hardback: ISBN 0-321-62089-9, ú35.00. International Journal of Climatology. 1998;18(5):579-80.

[2] Meadows DH, Meadows DL, Randers J, Behrens WW. The limits to growth. New York. 1972;102:27.

[3] Minger TJ, editor Greenhouse glasnost: the crisis of global warming: essays. Greenhouse/Glasnost: the Sundance Symposium on Global Climate Change,(USA), 1989; 1990: Ecco Press.

[4] Peet J. Energy and the ecological economics of sustainability: Island Press; 1992.

[5] Rose A. A global view of solar energy in rational units. physica status solidi (a). 1979;56(1):11-26.

[6] Shah A, Torres P, Tscharner R, Wyrsch N, Keppner H. Photovoltaic technology: the case for thin-film solar cells. science. 1999;285(5428):692-8.

[7] Turner JA. A realizable renewable energy future. Science. 1999;285(5428):687-9.

[8] Gong J, Liang J, Sumathy K. Review on dye-sensitized solar cells (DSSCs): fundamental concepts and novel materials. Renewable and Sustainable Energy Reviews. 2012;16(8):5848-60.

[9] Upadhyaya HM, Senthilarasu S, Hsu M-H, Kumar DK. Recent progress and the status of dye-sensitised solar cell (DSSC) technology with state-of-the-art conversion efficiencies. Solar Energy Materials and Solar Cells. 2013;119:291-5.

[10] Sharma K, Sharma V, Sharma S. Dye-sensitized solar cells: fundamentals and current status. Nanoscale research letters. 2018;13(1):381.

[11] O'regan B, Grätzel M. A low-cost, high-efficiency solar cell based on dye-sensitized colloidal TiO2 films. nature. 1991;353(6346):737.

[12] Ito S, Rothenberger G, Liska P, Comte P, Zakeeruddin SM, Péchy P, et al. High-efficiency (7.2%) flexible dye-sensitized solar cells with Ti-metal substrate for nanocrystalline-TiO 2 photoanode. Chemical Communications. 2006(38):4004-6.

[13] Yamaguchi T, Tobe N, Matsumoto D, Nagai T, Arakawa H. Highly efficient plastic-substrate dye-sensitized solar cells with validated conversion efficiency of 7.6%. Solar Energy Materials and Solar Cells. 2010;94(5):812-6.

[14] Cavallo C, Di Pascasio F, Latini A, Bonomo M, Dini D. Nanostructured semiconductor materials for dye-sensitized solar cells. Journal of Nanomaterials. 2017;2017.

[15] Grätzel M. Photoelectrochemical cells. nature. 2001;414(6861):338.

[16] Leung DY, Fu X, Wang C, Ni M, Leung MK, Wang X, et al. Hydrogen production over titania-based photocatalysts. ChemSusChem. 2010;3(6):681-94.

[17] Liu G, Gong J, Kong L, Schaller RD, Hu Q, Liu Z, et al. Isothermal pressure-derived metastable states in 2D hybrid perovskites showing enduring bandgap narrowing. Proceedings of the National Academy of Sciences. 2018;115(32):8076-81.

[18] Liu G, Kong L, Guo P, Stoumpos CC, Hu Q, Liu Z, et al. Two regimes of bandgap red shift and partial ambient retention in pressure-treated two-dimensional perovskites. ACS Energy Letters. 2017;2(11):2518-24.

[19] Wang X, Li Z, Shi J, Yu Y. One-dimensional titanium dioxide nanomaterials: nanowires, nanorods, and nanobelts. Chemical reviews. 2014;114(19):9346-84.

[20] Chandiran AK, Abdi-Jalebi M, Nazeeruddin MK, Grätzel M. Analysis of electron transfer properties of ZnO and TiO2 photoanodes for dye-sensitized solar cells. ACS nano. 2014;8(3):2261-8.

[21] Gillet M, Aguir K, Lemire C, Gillet E, Schierbaum K. The structure and electrical conductivity of vacuum-annealed WO3 thin films. Thin Solid Films. 2004;467(1-2):239-46.

[22] Zheng H, Tachibana Y, Kalantar-zadeh K. Dye-sensitized solar cells based on WO3. Langmuir. 2010;26(24):19148-52.

[23] Bae H, Yoon M, Kim J, Im S. Photodetecting properties of ZnO-based thin-film transistors. Applied Physics Letters. 2003;83(25):5313-5.

[24] Özgür Ü, Alivov YI, Liu C, Teke A, Reshchikov M, Doğan S, et al. A comprehensive review of ZnO materials and devices. Journal of applied physics. 2005;98(4):11.

[25] Zhang Q, Dandeneau CS, Zhou X, Cao G. ZnO nanostructures for dye-sensitized solar cells. Advanced Materials. 2009;21(41):4087-108.

[26] Biswas R, Roy T, Chatterjee S. Study of Electro-Optical Performance and Interfacial Charge Transfer Dynamics of Dye Sensitized Solar Cells Based on ZnO Nanostructures and Natural Dyes. Journal of Nanoelectronics and Optoelectronics. 2019;14(1):99-108.

[27] Costantino U, Marmottini F, Nocchetti M, Vivani R. New Synthetic Routes to Hydrotalcite-Like Compounds− Characterisation and Properties of the Obtained Materials. European Journal of Inorganic Chemistry. 1998;1998(10):1439-46.

[28] Oh J-M, Hwang S-H, Choy J-H. The effect of synthetic conditions on tailoring the size of hydrotalcite particles. Solid State Ionics. 2002;151(1-4):285-91.

[29] Daniel M, Desbat B, Lassegues J, Gerand B, Figlarz M. Infrared and Raman study of WO3 tungsten trioxides and WO3, xH2O tungsten trioxide tydrates. Journal of solid state chemistry. 1987;67(2):235-47.

[30] Sadek AZ, Zheng H, Breedon M, Bansal V, Bhargava SK, Latham K, et al. High-temperature anodized WO3 nanoplatelet films for photosensitive devices. Langmuir. 2009;25(16):9545-51.

[31] Hore S, Vetter C, Kern R, Smit H, Hinsch A. Influence of scattering layers on efficiency of dye-sensitized solar cells. Solar Energy Materials and Solar Cells. 2006;90(9):1176-88.

[32] Jin EM, Park K-H, Yun J-J, Hong CK, Hwang M-J, Park B-K, et al. Photovoltaic properties of TiO 2 photoelectrode prepared by using liquid PEG-EEM binder. Surface Review and Letters. 2010;17(01):15-20.

[33] Ko KH, Lee YC, Jung YJ. Enhanced efficiency of dye-sensitized TiO2 solar cells (DSSC) by doping of metal ions. Journal of colloid and interface science. 2005;283(2):482-7.

[34] Park K-H, Jin EM, Gu HB, Shim SE, Hong CK. Effects of HNO3 treatment of TiO2 nanoparticles on the photovoltaic properties of dye-sensitized solar cells. Materials Letters. 2009;63(26):2208-11.

[35] Qi B, Wang J. Fill factor in organic solar cells. Physical Chemistry Chemical Physics. 2013;15(23):8972-82.

[36] Grätzel M. Dye-sensitized solar cells. Journal of photochemistry and photobiology C: Photochemistry Reviews. 2003;4(2):145-53.

[37] Ito S, Liska P, Comte P, Charvet R, Péchy P, Bach U, et al. Control of dark current in photoelectrochemical (TiO 2/I−–I 3−) and dye-sensitized solar cells. Chemical Communications. 2005(34):4351-3.

[38] Noor S, Sajjad S, Leghari SAK, Shaheen S, Iqbal A. ZnO/TiO2 nanocomposite photoanode as an effective UV-vis responsive dye sensitized solar cell. Materials Research Express. 2018;5(9):095905.

[39] Adachi M, Sakamoto M, Jiu J, Ogata Y, Isoda S. Determination of parameters of electron transport in dye-sensitized solar cells using electrochemical impedance spectroscopy. The Journal of Physical Chemistry B. 2006;110(28):13872-80.

[40] Al-juaid F, Merazga A, Al-Baradi A, Abdel-wahab F. Effect of sol–gel ZnO spin-coating on the performance of TiO2-based dye-sensitized solar cell. Solid-State Electronics. 2013;87:98-103.

[41] Bedja I, Kamat PV, Hua X, Lappin A, Hotchandani S. Photosensitization of Nanocrystalline ZnO Films by Bis (2, 2 '-bipyridine)(2, 2 '-bipyridine-4, 4 '-dicarboxylic acid) ruthenium (II). Langmuir. 1997;13(8):2398-403.

[42] Sarker S, Ahammad A, Seo HW, Kim DM. Electrochemical impedance spectra of dye-sensitized solar cells: fundamentals and spreadsheet calculation. International Journal of Photoenergy. 2014;2014.

[43] Younas M, Gondal M, Dastageer M, Baig U. Fabrication of cost effective and efficient dye sensitized solar cells with WO3-TiO2 nanocomposites as photoanode and MWCNT as Pt-free counter electrode. Ceramics International. 2019;45(1):936-47.

[44] Wang Q, Moser J-E, Grätzel M. Electrochemical impedance spectroscopic analysis of dye-sensitized solar cells. The Journal of Physical Chemistry B. 2005;109(31):14945-53.

[45] Bisquert J. Chemical capacitance of nanostructured semiconductors: its origin and significance for nanocomposite solar cells. Physical Chemistry Chemical Physics. 2003;5(24):5360-4.

[46] Lim SP, Pandikumar A, Huang NM, Lim HN. Silver/titania nanocomposite-modified photoelectrodes for photoelectrocatalytic methanol oxidation. International Journal of Hydrogen Energy. 2014;39(27):14720-9.

[47] Buda S, Shafie S, Rashid SA, Jaafar H, Sharif N. Enhanced visible light absorption and reduced charge recombination in AgNP plasmonic photoelectrochemical cell. Results in physics. 2017;7:2311-6.

[48] Kim SG, Ju MJ, Choi IT, Choi WS, Choi H-J, Baek J-B, et al. Nb-doped TiO 2 nanoparticles for organic dye-sensitized solar cells. Rsc Advances. 2013;3(37):16380-6.

[49] Archana P, Gupta A, Yusoff MM, Jose R. Tungsten doped titanium dioxide nanowires for high efficiency dye-sensitized solar cells. Physical Chemistry Chemical Physics. 2014;16(16):7448-54.

This Page is intentionally left blank